

Semantic segmentation for recognition of epileptiform patterns recorded via Microelectrode Arrays in vitro

Gabriel Galeote-Checa¹, Gabriella Panuccio⁴, Ángel Canal-Alonso³, Teresa Serrano-Gotarredona¹, Bernabé Linares Barranco¹,

1 Instituto de Microelectrónica de Sevilla-IMSE, Centro Nacional de Microelectrónica, Consejo Superior de Investigaciones Científicas and Universidad de Sevilla, Sevilla, Spain

2 Enhanced Regenerative Medicine Lab, Instituto Italiano di Tecnologia, Genoa, Italy

3 Instituto de Investigación Biomédica de Salamanca-IBSAL, Consejo Superior de Investigaciones Científicas and University of Salamanca, Salamanca, Spain

4 Istituto Italiano di Tecnologia, Genoa, Italy

These authors contributed equally to this work.

* ggaleote@ieee.org

Abstract

Epilepsy is a prevalent neurological disorder that affects approximately 1% of the global population. Approximately 30-40% of patients do not respond to pharmacological treatment, leading to a significant negative impact on their quality of life. Closed-loop deep brain stimulation (DBS) is a promising treatment for individuals who do not respond to medical therapy. To achieve effective seizure control, algorithms play an important role in identifying relevant electrographic biomarkers from local field potentials (LFPs) to determine the optimal stimulation timing. In this regard, the detection and classification of events from ongoing brain activity, while achieving low power consumption through computationally unexpensive implementations, represents a major challenge in the field. To address this challenge, we here present two lightweight algorithms, the ZdensityRODE and the AMPDE, for identifying relevant events from LFPs by utilizing semantic segmentation, which involves extracting different levels of information from the LFP and relevant events from it. The algorithms' performance was validated against epileptiform activity induced by 4-aminopyridine in mouse hippocampus-cortex (CTX) slices and recorded via microelectrode array, as a case study. The ZdensityRODE algorithm showcased a precision and recall of 93% for ictal event detection and 42% precision for interictal event detection, while the AMPDE algorithm attained a precision of 96% and recall of 90% for ictal event detection and 54% precision for interictal event detection. While initially trained specifically for detection of ictal activity, these algorithms can be fine-tuned for improved interictal detection, aiming at seizure prediction. Our results suggest that these algorithms can effectively capture epileptiform activity; their light weight opens new possibilities for real-time seizure detection and, possibly, seizure prediction and control.

Author summary

Gabriel Galeote-Checa (Student Member, IEEE) is currently pursing his PhD in the Neuromorphic Systems research group at the Seville Microelectronics Institute (IMSE-CNM-CSIC), Seville, Spain, part of the Spanish National Research Council (CSIC) and the University of Seville (US). He is also involved in the EU H2020 FET-Proactive "HERMES" project, where he developed a flexible brain implantable device to treat epilepsy. His current research interest includes developing signal processing techniques for the detection and treatment of seizures via implantable stimulating devices. He is also working at Analog Devices Inc. as Biomedical Digital Signal Processing engineer.

Introduction

Epilepsy is a prevalent neurological disorder that affects approximately 1% of the global population [1]. The standard treatment of epilepsy relies on medical therapy; however, 30-40% of the patients respond poorly, if at all, to anti-epileptic drugs, falling into Drug Resistant Epilepsy (DRE) patients. Surgical removal of the epileptic focus is the current gold standard for those DRE patients. However, the success of the brain surgery highly depends on the accurate identification of the seizure focus. Brain stimulation has emerged as a promising and less radical alternative to ablative neurosurgery. In the recent years, there has been a rapid growth of brain implantable devices, driven by the recent contributions in wireless power transmission techniques [2–4], flexible electronics for implantable devices [3, 5], and device design miniaturization [6–8]. Among the diverse devices under pre-clinical and clinical research, NeuroPace (Mountain View, CA), which is the first FDA-approved responsive neurostimulation system for focal epilepsy, offers a median seizure reduction range of 50-70% across different studies [9]. Given the promising results in seizure suppression by responsive brain stimulation and the latest advances in brain implantable devices, the growth of these devices for the treatment of epilepsy is expected to accelerate in the next years. However, important aspects such as long-term viability, biocompatibility, power harvesting, and the need of more efficient and optimized algorithms make clinical results still improvable.

To operate effectively, brain stimulation devices should detect relevant electrographic biomarkers in order to determine the optimal stimulation timing and characteristics to suppress, or ideally prevent, seizure. Typically, local field potential (LFP) recordings are used for this purpose. Various biomarkers of interest, such as high-frequency oscillations (HFOs) [10–12], can be detected using embedded algorithms in the implantable device, allowing low latency real-time seizure suppression. In essence, the identification of those different biomarkers in the LFP signal would help to create decision schemes for closed-loop brain stimulation. However, the identification of electrographic biomarkers still remains challenging due to their diverse characteristics in terms of morphology, time/frequency features and their correlation with seizure events [12]. To address this challenge, various algorithms have been proposed, such as principal component analysis [13], linear support vector machine [14], approximate entropy [15], K-nearest neighbor and naïve bayes classification [14], feature extraction using support vector machines [16], or complex multi-feature-based decision schemes [17]. These consist of complex and computationally intensive algorithms hindering their potential for real-time operation. On the contrary, approaches such as phase synchronization in multichannel recordings [18], multilevel wavelet transform [19], Izhikevich neural networks [20], or Wiener algorithm [21], have been proven effective for real-time seizure detection implemented in hardware; however, most of them still require a significant amount of energy and memory to be

implemented in low-power and miniaturized systems.

At this juncture, we introduce an alternative methodology for identifying and categorizing epileptiform patterns within LFPs using a semantic segmentation approach. This approach enables to classify ictal and interictal events in LFP data based on their temporal and morphological characteristics, and to determine the current brain network state in real-time. Our primary goal is to achieve low computational complexity, making them suitable for hardware implementation, while allowing for the detection of relevant events based on various features in the LFP data. To this end, we have developed two novel algorithms and validated them via microelectrode array (MEA) recordings of epileptiform activity generated by mouse hippocampus-cortex (CTX) slices treated with the convulsant drug 4-aminopyridine (4AP), an established *in vitro* model of limbic ictogenesis [22], which offers several parallelisms with the most common type of DRE in humans, i.e., mesial temporal lobe epilepsy (MTLE), including the primary origin of ictal activity in the entorhinal cortex [23–26].

The two algorithms use different approaches; the first (ZdensityRODE) utilizes an adaptive z-score method, which uses a short-term memory strategy to provide a smooth detection of the brain's states. The second algorithm (AMPDE) uses scalogram-based peak detection and density estimation in the signal for extracting events of interest determined by their density of excitation. Both algorithms incorporate a post-processing technique with an accumulative look-forward time integration based on their density, and are capable of distinguishing among ictal discharges, interictal events, and baseline. The ZdensityRODE algorithm is significantly faster than the AMPDE, and more adaptable to long-term variations in signal amplitude and frequency, with low computational requirements but less accuracy in noisy environments. On the other hand, the AMPDE algorithm performs better in the presence of additive noise and can detect interictal events more effectively, despite requiring more computational resources and longer processing windows. To the best of our knowledge, this is the first proposal of such approach applied to LFPs recorded via MEA.

Materials and Methods

Microelectrode Array recording of epileptiform activity generated by brain slices

Horizontal hippocampus-cortex (CTX) slices (400 μm -thick) were obtained from 4-8 weeks old male CD1 mice. Epileptiform activity was acutely induced by treatment with 4-aminopyridine (4AP). Extracellular field potentials were acquired using a 6×10 planar MEA with TiN electrodes (diameter: 30 μm , inter-electrode distance: 500 μm) and a MEA1060 amplifier. Signals were sampled at 2 kHz, low-pass filtered at half the sampling frequency before digitization, and recorded to the computer's hard drive via the McRack software. All recordings were performed at 32°C. The full methodological details describing brain slice preparation and maintenance can be found in [27]. Animal procedures were conducted in accordance with the National Legislation (D.Lgs. 26/2014) and the European Directive 2010/63/EU, and approved by the Institutional Ethics Committee of Istituto Italiano di Tecnologia and by the Italian Ministry of Health (protocol code 860/215-PR, approval date 24/08/2015). Animals were daily monitored and euthanized under deep isoflurane anesthesia, assessing lack of reflexes upon feet, paws and tail pinch, thus being compliant with FELASA standards. The equipment for MEA recording and temperature control was obtained from Multichannel Systems (MCS), Germany. Fig. 1 highlights the electrode mapping relative to the brain slice position on the MEA, showing the different regions from where the LFP signals are recorded.

Dataset preparation

An overall validation dataset was generated from 7 brain slices. All records were annotated, identifying epileptiform events though a semi-automated approach, i.e., they were first detected via an automated algorithm, and then confirmed or modified as appropriate based on visual inspection. Events were labelled as ictal, interictal and baseline. This dataset constitutes our ground truth for the algorithm's validation. To ensure the homogeneity of the dataset, several inclusion criteria were established to signals in order to be used for the validation: i) uniform sampling at a rate of 2 kHz to standardize disparate sample rates and ensure consistent recording precision; ii) records from the electrodes within the parahippocampal cortex (See Fig. 1).

Experimental design: Parameter Search and Optimization Procedure

All records were maintained for training in different scenarios, similar to online operation, under low and high SNR conditions, to avoid a possible overfitting the algorithm. Table 1 summarizes the dataset characteristics for this experiment. Algorithms were trained with an optimization matrix including variations for each of the parameters of the algorithms. The complete set of combinations is described in Table 2, where the parameter search frame is detailed. The experimental protocol devised for this study is depicted in Figure 2. The dataset is divided into 70-30 test-validation split. After running the algorithms in the training dataset, the best 10 scores were averaged. For recordings with low Signal-to-Noise Ratios (SNR) (< 20 dB), parameters were further fine-tuned before validation stage, to improve the accuracy. The experiments were conducted on a supercomputer provided by the Centro Informatico Cientifico de Andalucia (CICA) in Andalusia, Spain, comprising over 50 nodes with nearly 600 cores interconnected via Infiniband DDR at 20 Gbps.

Table 1. Brain slice MEA electrophysiology dataset description.

Parameter	Value
Number of signals	68
Brain region	Parahippocampal cortex
Sampling rate	2 kHz
Total recording time (Average)	1800 s
Signal-to-noise ratio (SNR)	from 20 ± 10 dB
Electrode type	Microelectrode array (MEA)

Table 2. Algorithm optimization experiment matrix. Optimization matrix for the two algorithms. Combinations for each of the parameters of the algorithm and experiments.

Algorithm	Optimization Parameters
ZDensityRODE	Threshold $[\sigma]$: 4, 5, 6
	Delta convolutional filter [seconds]: 3, 4, 5
	Lag [seconds]: 0.125, 0.25, 0.5
AMPD	Threshold $[\sigma]$: 3, 4, 5, 6
	Delta Time Integration $[\sigma]$: 1.5, 2, 2.5

Z-score Density-based Robust Outlier Detection Estimation (ZDensityRODE)

Assuming that the LFP signal is primarily composed of baseline, we could presume that any outlier in the signal's trend might be of interest. Subsequently, through an analysis of its temporal duration, proximity to other outliers, and magnitude, we could, to some extent, estimate the type of event it may represent. The ZdensityRODE algorithm is based on the statistical Z-score test to measure the variability of data points within a data trend using the historic mean and standard deviation of the distribution to evaluate outliers with regard to the distribution characteristics. The Z-test has been proven to be a confident measure of variability when it comes to detect outliers [28]. It can be implementable in real time since it can work sample by sample with consideration of historical data. Given the z-score combined with historic mean and standard deviation; outliers can be detected with much higher detection performance. Once they are identified in the time series, the spike density of the events is integrated and evaluated to fall into one or another kind of event.

This algorithm can be configured using four parameters lag (λ), threshold (τ), influence (i), and delta (Δ). The lag parameter determines how many past samples are considered for computing the historic average and standard deviation. A longer lag provides stability against rapid changes but increases memory load, while a shorter lag enables quicker adaptation to new information but increased variability. The threshold parameter sets the z-score level at which a data point is deemed significant, allowing for more precise detections based on signal features like the SNR. The influence parameter (ranging from 0 to 1) controls the weight given to incoming samples when recalculating averages and standard deviations, with 0 disregarding new data and 1 providing high adaptability. Lastly, the delta parameter defines the refractory time between peaks, crucial for pattern classification during post-processing analysis of peak candidates. This parameter regards the duration of events and their separation in time. The algorithm workflow is depicted in Figure 3.

The algorithm starts with a training stage, in which during the first λ samples, the algorithm does not provide any detection but fills the buffers and calculate the initial trend of the data. Only a Notch filter at 50 Hz to remove powerline noise (here, 50 Hz) is used in the signal conditioning stage. During this stage, that lasts as long as the lag time parameter, initial mean (μ) and standard deviation (σ) buffers are filled (See Fig. 3). Once the algorithm is trained, it starts the operation mode by processing each incoming sample in three steps: (i) a z-score test relative to μ and σ , which are estimated values from previous samples in the signal (Eq. 1); (ii) local maxima evaluation by first-derivative test (Eq. 2); (iii) refractory period evaluation.

$$z = \frac{x_n - \mu}{\sigma} \quad (1)$$

$$x_{n-1} < x_n \oplus x_{n+1} < x_n \quad (2)$$

Where x_n is the current sample, μ is the historic mean and σ is the historic standard deviation. Both historic μ and σ are implemented as FIFO, storing the λ last samples and recalculated on each sample with the influence parameter depending on the result of the z-score. On positive results of the z-score, which means that the peak is prominent and significant, the μ and σ filters are updated following the expression in Eq. 3. A positive result of the z-score indicates that the current incoming value is above the normal trends, thus, the historical data is updated based on the influence defined by ι . If the z-score test is negative, implying noise or irrelevant information, the filters μ and σ are updated without considering the influence parameter, that is providing less importance to the current sample.

$$\bar{x}_n < \iota * \bar{x}_i - (1 - \iota) * \bar{x}_{i-1} \quad n = 0, 1, \dots, \lambda \quad (3)$$

Upon detecting outliers, these are transformed into intervals. The peak density estimation consists on measuring both, the extent of an event and the proximity with its next peak. If one or more peaks are within the integration time Δ , the detection window is extended until peaks are separated further than the refractory time. Once the rule is not satisfied, the integration is stopped and the interval is classified. The interval classification is determined by the characteristics of the event, i.e. using the duration of the interval and the spike density.

Automatic multiscale-based peak detection (AMPDE)

The scalogram technique has demonstrated its efficacy and robustness in the context of peak detection, particularly in scenarios characterized by noise and diverse peak morphologies [29]. Through a scalogram-based multiscale decomposition employing various windows and subsequent row-wise peak identification, the algorithm exhibits remarkable performance in detecting pertinent events, as demonstrated by Scholkmann et al. [30]. The implemented algorithm encompasses six distinct stages: the Signal Conditioning stage, the calculation of Local Maxima Scalogram (LMS), the determination of the optimal scale, LMS rescaling, peak detection, and the estimation of peak density for brain activity pattern classification. A comprehensive block diagram of the algorithm is provided in Figure 4, offering a visual representation of each step within the processing pipeline and input/output (I/O) delineation.

Let us consider now an univariate signal, $x(i)$, with N uniformly sampled points, $1 \leq i \leq N$, containing periodic or quasi-periodic peaks. The first step involves preprocessing the input signal to remove the offset, and eliminate the power line interference (Here, 50 Hz) by applying a notch filter with a quality factor of 90. Then the LMS is computed by analyzing all input values ($x = x_1, x_2, x_3, x_4, \dots, x_n$) using a moving window approach. The LMS uses the scalogram for detection peaks in the time series. The scalogram is the signal's frequency distribution over time, analogous to spectrogram. This representation enables the extraction of significant features such as peaks, edges, and patterns. In this work, we are interested on the detection of peaks and this representation provides trustworthy measure of relevant events and their frequency components. To obtain the

LMS matrix, the signal x is first detrended by subtracting the least-squares fit of a straight line from x . That removes the long term memory of the signal and avoids adding carried trends into the current portion of signal where the scalogram has to be computed. Next, the signal is averaged with a moving window average filter with varied lengths. The window length w_k is varied from 2 to L , $w_k = 2k$, $k = 1, 2, \dots, L$, where L is defined as $L = \lceil \frac{N}{2} \rceil - 1$. This is performed for every scale k and for $i = k + 2, \dots, N - k + 1$.

$$m_{k,i} = \begin{cases} 0 & x_{i-1} > x_{i-k-1} \wedge x_{i-1} > x_{i+k-1} \\ r + \alpha & \text{otherwise} \end{cases} \quad (4)$$

where r is a uniformly distributed random number in the range $[0, 1]$ and α a constant factor ($\alpha = 1$). Each $m_{k,i}$ element is formed as the value $r + \alpha$ for $i = [1, 2, \dots, k + 1]$ and for $i = [N - k + 2, \dots, N]$. The result of performing all those operations for each of the windows is a matrix $L \times N$ defined as Eq. 5. Each row in this matrix corresponds to a window length w_k . It represents the local maxima scale of the signal for each window. To gather information about the scale-dependent distribution of zeros (and consequently local maxima) in the signal segment, a row-wise summation is performed for each LMS level, as shown in Eq. 6.

$$M = \begin{bmatrix} m_{1,1} & \cdots & m_{1,N} \\ \vdots & \ddots & \vdots \\ m_{L,1} & \cdots & m_{L,N} \end{bmatrix} \quad (5)$$

$$\gamma_m = \frac{1}{L} \sum_{k=1}^L m_{k,m} \text{ for } k \in 1, 2, \dots, L \quad (6)$$

The vector $[\gamma_1, \gamma_2, \dots, \gamma_L]$ contains information about the distribution of zeros that is scale dependent, including the local maxima. The next step uses a parameter λ to reshape the LMS matrix M by removing all elements $m_{k,i}$ for which $k > \lambda$ holds. It allows one to reshape the LMS matrix leading to the new $\lambda \times N$ -matrix $(r_{k,i})$, for $i \in 1, 2, \dots, N$ and $k \in 1, 2, \dots, \lambda$. From the matrix, the peak detection is performed by: (i) Calculating the column-wise standard deviation of the matrix according to Eq. 7 and (ii) Finding all indices i that satisfy $\sigma_i = 0$. These values are stored in the vector $\hat{p} = [\hat{p}_1, \hat{p}_2, \dots, \hat{p}_{\hat{N}}]$ with \hat{N} being the total number of detected peaks of the signal x .

$$\sigma_i = \sqrt{\frac{1}{\lambda} \sum_{k=1}^{\lambda} (m_{k,i} - \gamma_k)^2} \text{ for } k \in 1, 2, \dots, N \quad (7)$$

In the final step, an estimate of the peak density is performed by searching for peaks in a Δ time and extending the detection interval if one or more peaks are within that Δ until peaks are separated further than the refractory time, similarly as in ZdensityRODE algorithm. For each detected peak, the algorithm searches for additional peaks within the next time interval defined by Δ . This search continues until no further peaks are found. This peak-centered counting process emphasizes the density of peaks and extends in time as long as the region of heightened excitability persists.

Performance metrics

In semantic segmentation problems, assessing the performance of an output model falls on its concordance with the reference model. In other words, for the algorithm, a positive

detection corresponds to a sequence of labels that collectively constitute a semantic field, or, in the context of the present work, a specific type of event in the LFP signal. Comparing reference and output annotations require an approach based on set theory. As mentioned, a true positive (TP) detection requires determining the intersection between the time intervals associated with the detected event and the reference event. The degree of overlap between these events settles a robust metric for measuring algorithm performance. The reference and output interval intersection is computed as Eq. 8. Dividing the coincidence segment by the reference segment, the coincidence ratio is obtained, which quantifies the degree of overlap between the two events (refer to Eq. 9).

$$\text{Coincidence Sequence} = [r_n, r_{n+i}] \cap [y_m, y_{m+j}] \quad (8)$$

$$\text{Coincidence Ratio} = \frac{\min(r_{n+i}, y_{m+j}) - \max(r_n, y_m)}{r_{n+i} - r_n} \quad (9)$$

Where y and r are an output and reference intervals of bounds $[n, n+1]$ and $[m, m+j]$ respectively. Both are defined as vectors, since they are a sequence of labels that together constitute events, for each of the samples of the signal. Here, a true positive detection is considered when more than the 80% of the output event coincides with the reference events and the length does not exceed a 50% on the boundaries of the reference event. Similarly, a False positive (FP) occurs when a event is detected where no reference event is found. False negative falls for a missed detection, either not detected or not sufficient for being classified as TP. In this context, Precision (P +) measures the proportion of true positives over false positives, quantifying how well the output events match clinical annotations (Eq. 10). Recall (Re) gauges the reliability of the algorithm's actual detections, signifying the fraction of positive patterns correctly classified (Eq. 11). The F-measure, also known as the F1 score, strikes a balance between precision and recall, offering a unified score to represent their trade-off (Eq. 12). We also employ the Jaccard/Tanimoto similarity index (Jaq) to assess the degree of overlap between detected events by comparing reference and output vectors (Eq. 13) [31]. These metrics provide comprehensive insights into the algorithm's performance.

$$\text{Precision} = \frac{TP}{TP + FP} \quad (10)$$

$$\text{Recall} = \frac{TP}{TP + FN} \quad (11)$$

$$\text{F Score} = 2 \times \frac{\text{Precision} \times \text{Recall}}{\text{Precision} + \text{Recall}} \quad (12)$$

$$\text{Jaccard index} = \frac{|A \cap B|}{|A \cup B|} \quad (13)$$

A Multi-Criteria Decision Analysis (MCDA) is proposed, to combine precision, recall, jaccard index and f-measure to extract a more comprehensive score of the algorithm performance. There is no clear indication as to which metric should be prioritized, nor is there a preferred metric for assessing such kinds of problems. For instance, in [7, 18, 32], recall is used as a fundamental metric for seizure detection, while in [14, 15, 33–35] precision is used as key indicator. Sensitivity is also employed by [16, 34–36] or specificity

in [35,36]. In this work, special relevance is given to the precision of ictal events. However, the Jaccard index is also added to enhance precision over interval intersection. The recall for ictal events is equally important to ensure reliable detection. Regarding interictal events, equal relevance is given to precision and recall but much lower than ictal events since their relevance is relative but ictal events are the most important patterns to detect. The scoring function, presented in Eq. 14, reflects the prioritization of ictal event detection over interictal detection. A higher weight is assigned to ictal detection, aligning with its relative importance in the scoring function. During the train stage, the weight given to each of the metrics define how the algorithm is prepared for the online operation mode, thus special attention must be focus on this stage to prepare the algorithm for the required task.

$$\begin{aligned}
 \text{Score} = & 0.6 \times \text{Precision}_{\text{ictal}} + 0.2 \times \text{Jaccard}_{\text{ictal}} + \\
 & 0.1 \times \text{Recall}_{\text{ictal}} + 0.05 \times \text{Precision}_{\text{interictal}} + \\
 & 0.05 \times \text{Recall}_{\text{interictal}}
 \end{aligned} \tag{14}$$

where $\text{Precision}_{\text{ictal}}$ is given a weight of 60% and $\text{Jaccard}_{\text{interictal}}$ is given a weight of 20%. The metric $\text{Recall}_{\text{ictal}}$ is given 10%, $\text{Precision}_{\text{interictal}}$ is given a 5 % and $\text{Recall}_{\text{interictal}}$ a 5 %. Including more metrics for the interictal class was devised, but it may sparse the scoring function and produce some wrong score because there are many cases in which the recall for interictal class could be very low, especially if the SNR of the signal is low.

Results

LFP signal characteristics vary remarkably among brain regions. This work focuses on LFP recorded from the CTX, which is the primary site of ictal onset in the in vitro model of limbic ictogenesis used in this work [22], consistent with what reported in several human studies [17, 27, 37, 38]. Fig. 5A illustrates the power spectral density (PSD) plot of epileptiform activity recorded from the entorhinal cortex. The frequency features of these signals was described in previous research, where the meaningful content of the CTX signal spectrum was shown to lie within 0.5 to 30 Hz, with additional relevant components at 350-390 Hz and around 650 Hz [39].

In terms of morphology, ictal events are continued high-amplitude, high-frequency discharges observable during seizures, whereas interictal epileptiform discharges, observed between ictal activity, are brief electrographic events that manifest in various forms like single spikes, spike bursts, or oscillations of low/high frequency [40]. The baseline section represents the signal's noise floor, denoting the absence of epileptiform events. This state is typified by a low-amplitude, uniformly shaped signal that remains relatively stable over time. In terms of their frequency characteristics, ictal events concentrate their spectral power within the frequency range of 0.5 to 30 Hz. On the other hand, interictal events exhibit diverse natures, leading to variations in their spectral representation across different event types. Notably, High-Frequency Oscillations (HFOs), which are often found within interictal epileptiform discharges [12, 41], span a range of 80 to 500 Hz [41, 42]. Authors have used those characteristics in time and frequency to detect ictal, interictal and baseline events. Some of those indicators for differentiating among those events are (i) morphological features like spike-maximum amplitude, spike slope, absolute mean of windowed events, and successive spike density [7,14,43,44]; (ii) spectral

features such as power content across different frequency bands [7, 15, 18, 44–46]; and (iii) statistical features like variations in median and variance [7, 14, 21], or kurtosis and skewness analysis [43].

In this work, only temporal characteristics were employed for the differentiation of the three categories, to achieve reduced computational cost. The events were categorized by their duration and amplitude, but also density within an integration window. From the 7 brain slices used for the experiments, a total of 68 records (30 minutes each) were captured, from different electrodes, satisfying the inclusion criteria previously described. The process resulted in 2457 different parameter configurations. An example of the two algorithms performance is shown against a sample signal and its reference annotations from the dataset in Fig. 6. Our results demonstrate a high performance of the algorithms in detecting ictal events with high recall and high precision (see Fig 7). To ensure a comprehensive evaluation of the algorithms performance, a multicriteria decision analysis was conducted considering precision, sensitivity, f1-score and jaccard index with different weights for ictal and interictal events depending on which detection is prioritized. Both algorithms consistently achieved high scores, with more than 90% in the global score indicating its robustness and reliability in detecting ictal events, but also interictal events with a precision higher than 50%, but lower sensitivity and jaccard index. ZdensityRODE achieved a precision of $P+ = 93\%$ and recall $Re = 93\%$, with a Jaccard index (Jaq) of 86% and F1-score of 91% for ictal event detection. However, for interictal events, it achieved a precision of $P+ = 42\%$ and recall of $Re = 45\%$. On the other hand, the AMPDE algorithm achieved a $P+ = 96\%$ and $Re = 90\%$, with $Jaq = 86\%$ and F1-score of 92% for ictal event detection, and a $P+ = 54\%$ and $Re = 33\%$ for interictal events. The algorithm was trained giving greater importance to ictal detection, thus reflecting a lower performance for interictal detection. Table 3 provides information about the results for each recording session and for each evaluation metric.

Table 3. Average evaluation metrics. This table shows the averaged results for each experimental session in the validation dataset. On the top, the results for ZdensityRODE algorithm and on the bottom, for AMPD algorithm.

Session	precision Ictal	precision Interictal	recall Ictal	recall Interictal	jaccard Ictal	jaccard Interictal	F Measure Ictal	F measure Interictal	score
20170420	0.82	0.49	1.00	0.52	0.82	0.36	0.89	0.49	0.80
20170505	1.00	0.82	0.85	0.89	0.83	0.74	0.92	0.85	0.93
20170606	1.00	0.40	1.00	0.50	1.00	0.40	1.00	0.44	0.94
20170926	1.00	0.49	0.92	0.38	0.92	0.33	0.95	0.41	0.92
20171005	1.00	0.17	0.75	0.24	0.75	0.11	0.83	0.20	0.84
20171107	0.71	0.59	1.00	0.64	0.71	0.26	0.75	0.38	0.73
20171128	1.00	0.00	1.00	0.00	1.00	0.00	1.00	0.00	0.90
Average	0.93	0.42	0.93	0.45	0.86	0.31	0.91	0.40	0.87

Session	precision Ictal	precision Interictal	recall Ictal	recall Interictal	jaccard Ictal	jaccard Interictal	F Measure Ictal	F measure Interictal	score
20170420	0.98	0.69	0.91	0.18	0.90	0.16	0.94	0.27	0.93
20170505	0.92	0.70	0.92	0.30	0.84	0.29	0.91	0.37	0.88
20170606	1.00	1.00	0.80	1.00	0.80	1.00	0.89	1.00	0.94
20170926	0.95	0.34	0.94	0.32	0.90	0.25	0.95	0.33	0.88
20171005	0.91	0.48	0.92	0.21	0.83	0.17	0.91	0.29	0.85
20171128	1.00	0.00	0.88	0.00	0.88	0.00	0.94	0.00	0.86
Average	0.96	0.54	0.90	0.33	0.86	0.31	0.92	0.38	0.89

It is relevant to note that the SNR substantially influences the algorithmic performance. To address this possible issue, we used Pearson correlation analysis to examine the correlation between the algorithm score and the SNR. This analysis resulted in a

Pearson's correlation coefficient of $r=0.7$ within the training dataset and $r=0.4$ within the validation dataset. This correlation is observable in Fig. 7, where A) and C) represent the corresponding results for each dataset, while B) and D) depict the SNR ranges for each recording session. Signals with higher SNR reported higher performance. This variability is akin to selecting the MEA channels based on their anatomical position and assessing signal quality for SNR threshold compliance. Despite this variability, the algorithm exhibits an outstanding overall performance. Besides, the correct choice of parameters highly determine the algorithm performance as illustrated in Fig. 7 E and F.

Discussion

In this work we have proposed a novel approach for detection of epileptiform activity, based on semantic segmentation of LFP signals. Namely, we have designed two algorithms: ZdensityRODE employs statistical variance and average analyses, through a Z-score test, of the signal with several memory buffers; the AMPDE uses successive wavelet decompositions in a scalogram based matrixial peak detection to efficiently extract prominent peaks. Both algorithms incorporate a strategy of spike density estimation with a forward lookup integration to classify different events. The two algorithms were validated using epileptiform activity recorded via MEA from 4AP-treated rodent brain slices. Both ZdensityRODE and AMPDE algorithms achieved impressive ictal detection performance (Precision $\gg 90\%$, Recall $\gg 90\%$, F1-score $\gg 90\%$). Specifically, ZdensityRODE achieved a precision of 93% and sensitivity of 93%, whereas AMPDE achieved a precision of 96% and sensitivity of 90%. It is relevant to highlight that both algorithms perform a semantic segmentation task, thus, they can also detect interictal events.

In the effort to improve epilepsy diagnosis and treatment, several algorithms have been proposed for the detection of seizures in LFP. In [18], a magnitude and phase synchronization between electrodes could achieve a 66% true positive rate (TPR). Yoo et al [7], used SVM yielding a TPR of 82.7% for seizure classification. Shoeb et al [47] proposed a machine learning technique through feature vector for detection of seizures, achieving a 96% of sensitivity and a 2/24h FPR. Kurtosis, skewness and coefficient of variation from decimate Discrete Wavelet Decomposition was proposed by [48], achieving a precision of 92.66%. Ronchini et al [35], uses entropy- and-spectrum features for seizure detection algorithm, boasting an accuracy of 97.8%. In [45], seizure detection is done by decimate discrete wavelet decomposition and interquartile range and mean absolute deviation, obtaining a precision of 84.2%, sensitivity of 98.5% and latency of 1.76 seconds.

Table 4 summarizes the performance and algorithmic approaches for the works mentioned above in a comparative table. Many of those implementations were tailored around the single patient rather than being designed as patient-agnostic approaches. In this regard, there is a great debate on the advantages of one approach over the other [49]. On the one hand, personalized algorithms offer a broad range of adjustable parameters and involve a training process; on the other hand, patient-agnostic approaches employ a fixed-parameter detector without the need for additional training [49, 50]. This decision requires a trade-off between detection accuracy, simplicity, and speed. Following any of those approaches determines the accuracy of the algorithm but also its applicability to different patients and scenarios. In this study, we have prioritized the development of a seizure detection method that is not patient-specific, but implements minimum levels of customization for improved accuracy.

Table 4. Comparative analysis of MEA event detection algorithms. This table compares several algorithms for event detection, i.e. seizure and/or interictal events.

Paper	Year	Algorithm approach	Precision [%]	Sensitivity [%]
[36]	2016	NLSVM	-	95.7
[18]	2011	CORDIC	-	66
[7]	2013	SVM	-	82.7%
[15]	2018	Approximate Entropy + FFT	97.8	-
[14]	2015	KNN, SVM, Naive bayes, logistic regression	80	95.24
[16]	2020	SVM	-	100
[33]	2018	CNN	-	79.2
[35]	2022	STDP	97.8	85.4
[47]	2010	Feature vector extraction	-	96
[48]	2012	Kurtosis, skewness and coefficient of variation from the decimate DWT	-	100
[4]	2013	Single window count, Multiple window count, spectral entropy	-	94
[45]	2014	Decimate DWT and interquartile range and mean absolute deviation	84.2	98.5
ZdensityRODE	2023	Z-score test with memory buffering strategy	(ictal) 93, (interictal) 42	93
AMPDEC	2023	Multiscale peak detection through DWT	(ictal) 96, (interictal) 54	90

NLSVM: Non-Linear support vector machines

CORDIC: Coordinate rotation digital computer

FFT: Fast fourier transform

SVM: Support vector machines

STDP: Spike-Timing Dependent Plasticity

DWT: Discrete wavelet transform

CNN: Convolutional neural networks

The identification of relevant biomarkers in LFP signals poses a significant challenge in the epilepsy field, because of the complex dynamics and different morphologies of ictal and interictal events. Further, the SNR significantly influences the performance of event detection algorithms. In various applications, signal quality assessment techniques improve algorithm performance by preventing unnecessary processing under unfavorable conditions [51, 52]. In this work, a low SNR particularly challenged accurate detection by ZdensityRODE, whereas AMPDEC proved robust to additive noise, excelling in analyzing frequency bursts. The first step for inferring a seizure onset or creating a seizure prediction scheme is to gather data from the LFP signal. Then, through clinical guidelines, the seizure onset can be predicted with a high accuracy. The aim of this work was to introduce a new approach to the field through two semantic segmentation algorithms, that enables the identification of brain states during real-time operation, helping to generate more information for seizure detection and control.

Conclusion

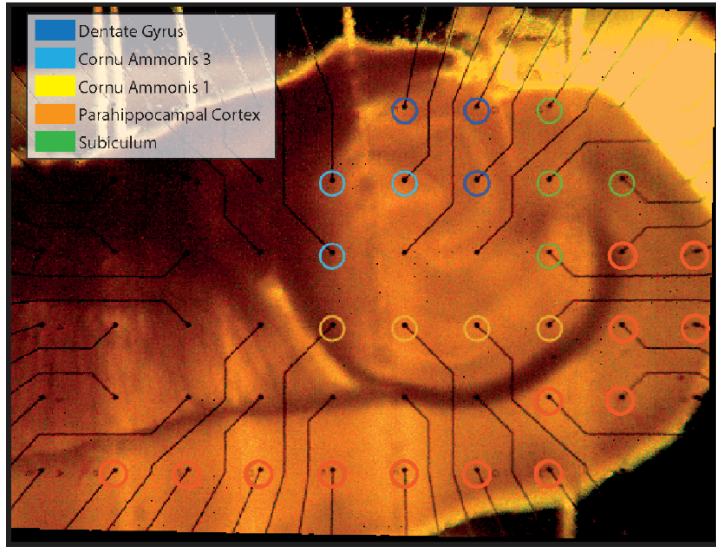
The detection of pathological biomarkers in LFP signals recorded from epileptic patients is fundamental for the timely detection (or better, prediction) of seizures to improve brain stimulation strategies for epilepsy treatment. Furthermore, such electrographic biomarkers can provide supplementary information to improve our understanding of brain states related to epilepsy. Both the ZdensityRODE and AMPDEC have demonstrated their efficient biomarkers detection with a lightweight and non-computationally demanding processing, by using temporal features such as spike amplitude, duration and density.

Thus, the LFP semantic segmentation proposed here introduces a new powerful approach to the field of seizure detection and control that promises to help identify relevant from non-relevant information within LFP signals for improved brain stimulation strategies for epilepsy treatment. We believe that these algorithms can provide a meaningful new perspective to the field and help to start a new subset of algorithms for epileptiform event classification and seizure prediction in real time, along with efficient offline operation.

Supporting information

Figures

A)



B)

Microelectrode Recordings

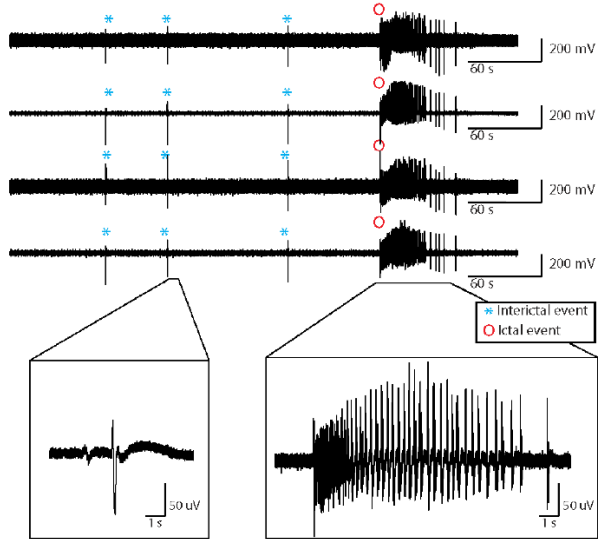


Figure 1. Epileptiform patterns recorded from hippocampus-CTX slices via MEA. (A) Mouse brain slice placed on a planar 6 x 10 MEA grid (grid separation of 500 μ m). Electrodes are grouped by their position in the brain region. (B) Four representative multichannel samples extracted from CTX region electrodes. Interictal events and Ictal events are marked in the signal for better understanding.

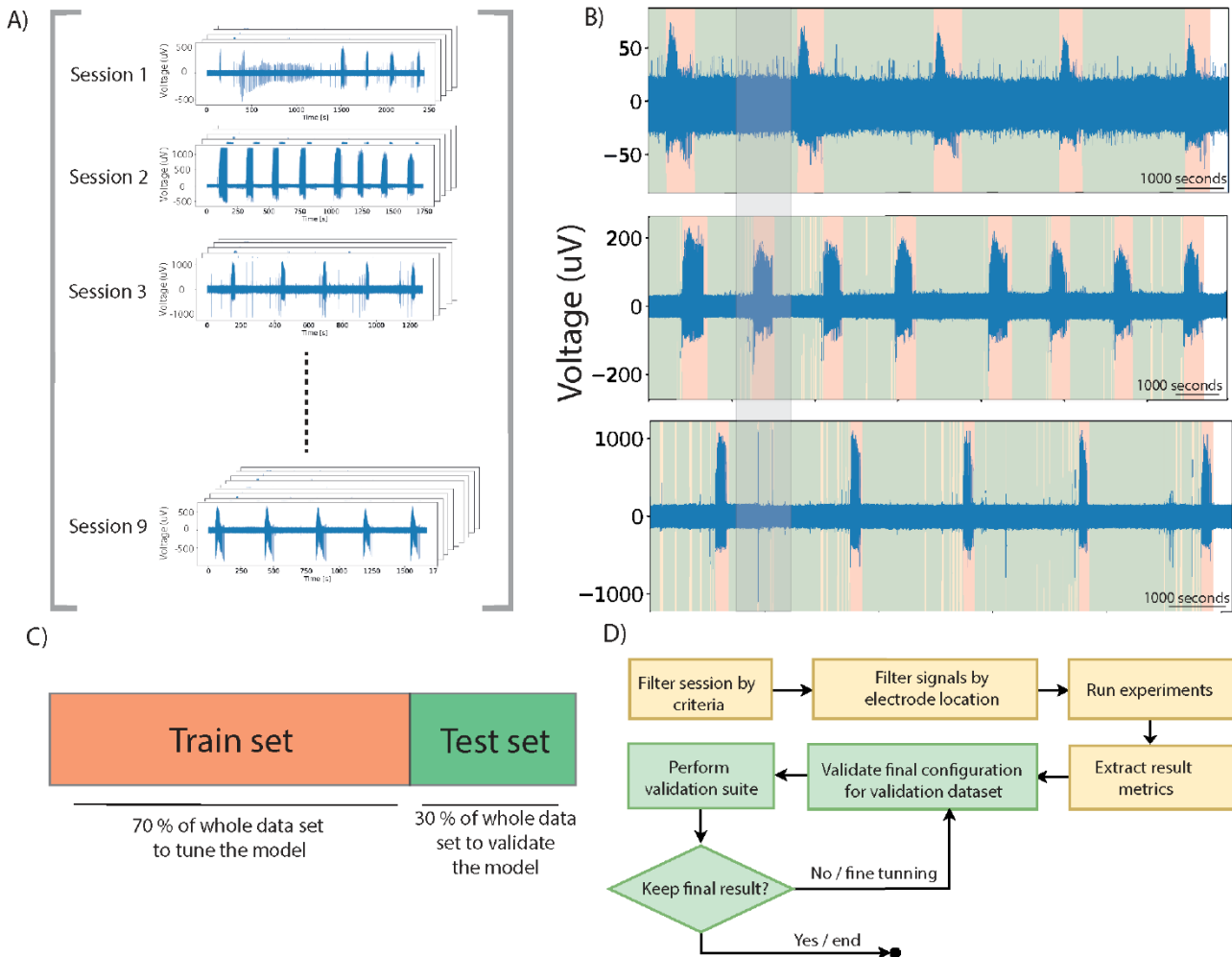


Figure 2. Experiment design description A) Compendium of MEA recording datasets. B) Annotated signals showing the three different patterns, highlighted in different colors: baseline (green), interictal (yellow) and ictal (red). C) Test/train split of the dataset. D) Experiment design block diagram with the sequence of stages chosen for the experimental stage.

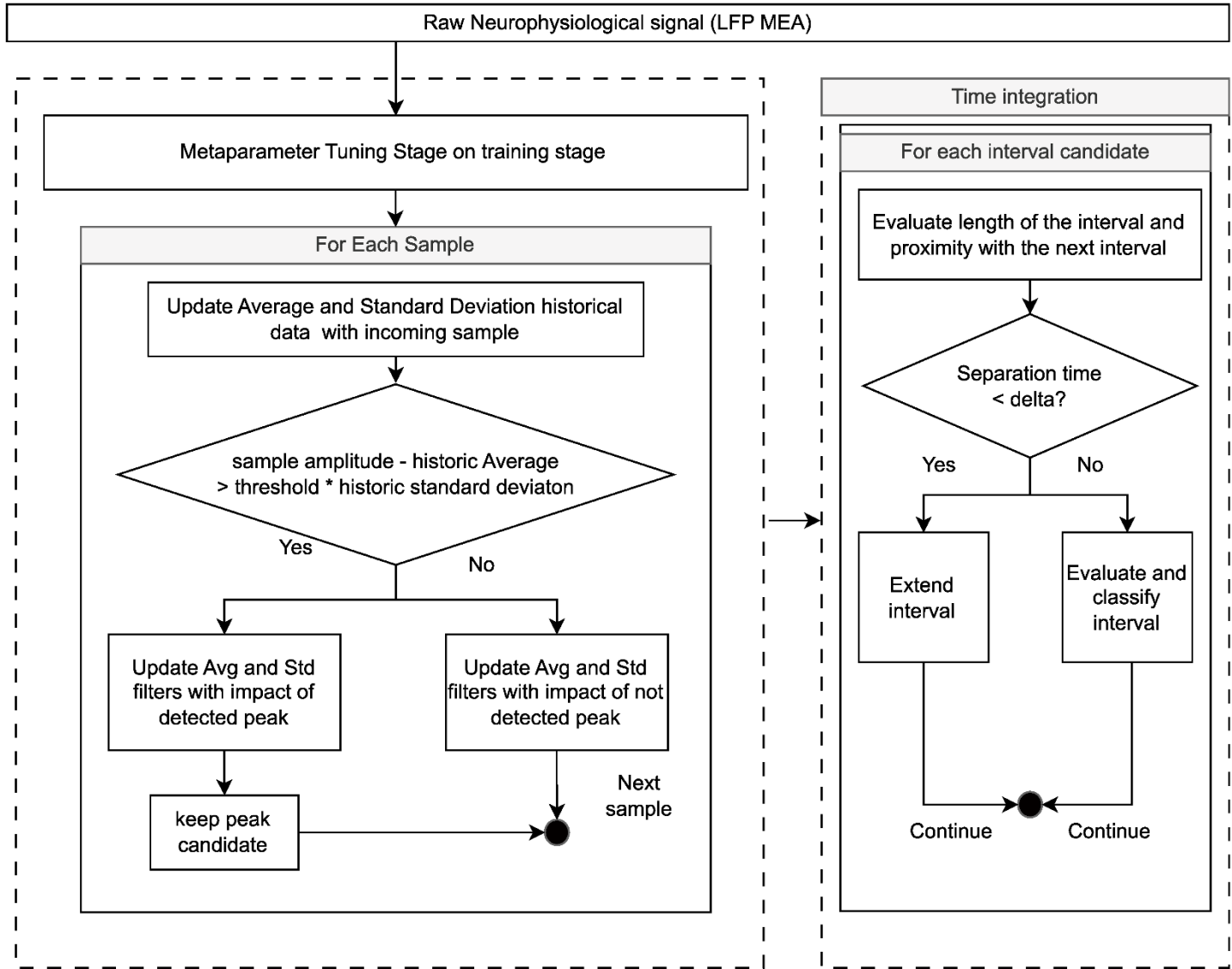


Figure 3. ZDensityRODE algorithm flowchart. Block diagram with the workflow of the Z-score Density-based Robust Outlier Detection Estimation algorithm.

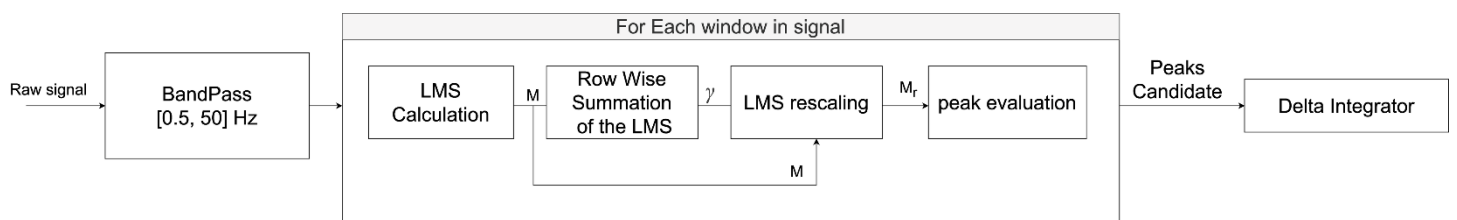


Figure 4. AMPD enhanced algorithm flowchart. Block diagram with the workflow of the Automatic multiscale-based peak detection (AMPDE) algorithm. At the first stage, a bandpass filter between 0.5 and 50 Hz is set. Then a LMS calculation is performed for each window in the signal. A summation of each row in the LMS returns the vector, which after a rescaling obtains the final vector of peaks candidate, filtered with an evaluation method to identify the peaks on the vector.

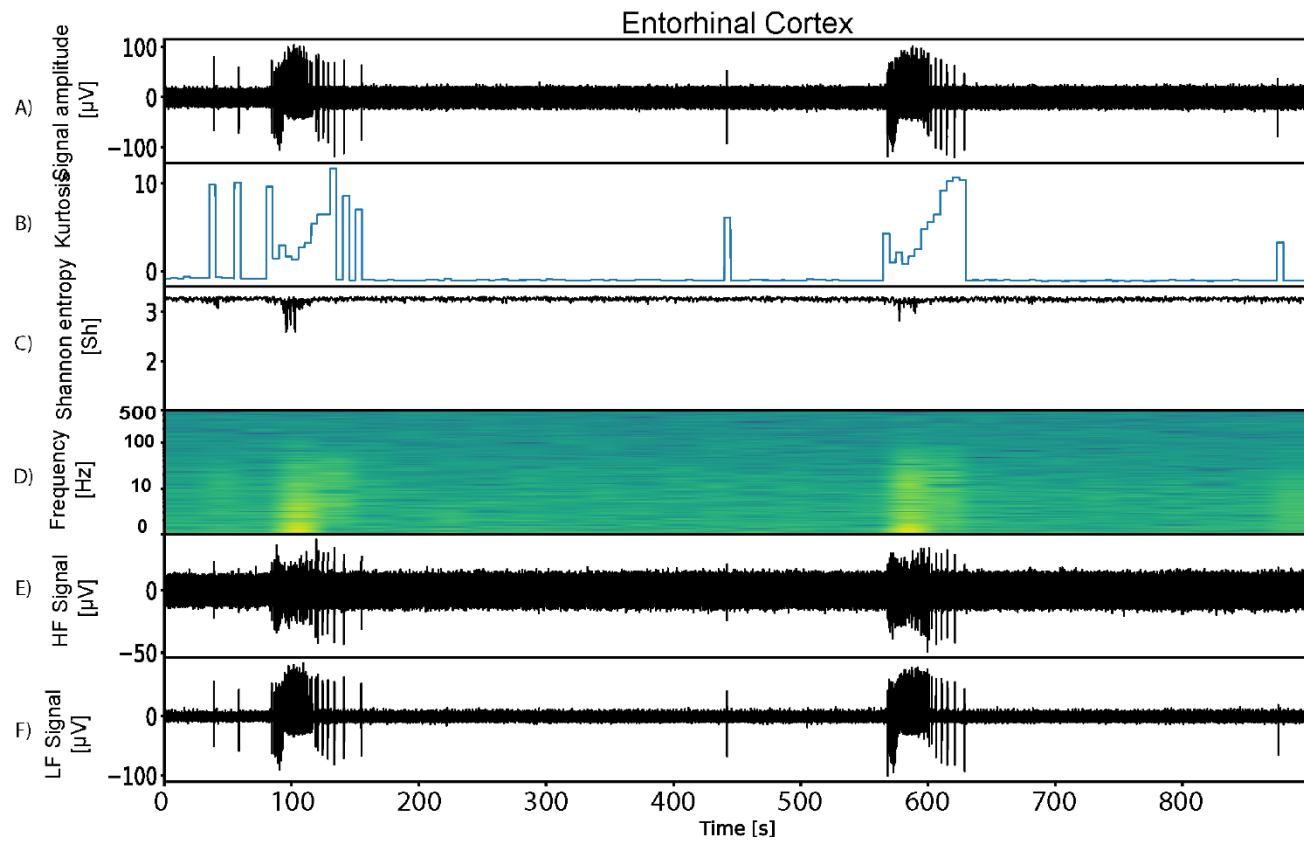


Figure 5. Parahippocampal LFP signal recorded via MEA A) epileptiform activity recorded from the entorhinal cortex (EC). The entorhinal cortex generates recurrent ictal-like discharges as well as slow interictal-like events; B) Kurtosis, a measure of the fourth momentum of the mean and standard deviation in chunks of 5 seconds; C) Shannon entropy, highlighting the variance and complexity of both signals over time. D) spectrogram of the entorhinal cortex, with the distribution of frequencies over time; E) shows the signal after high-pass filtering at $\geq 300\text{Hz}$; F) shows the signal after low-pass filtering at $\leq 300\text{Hz}$.

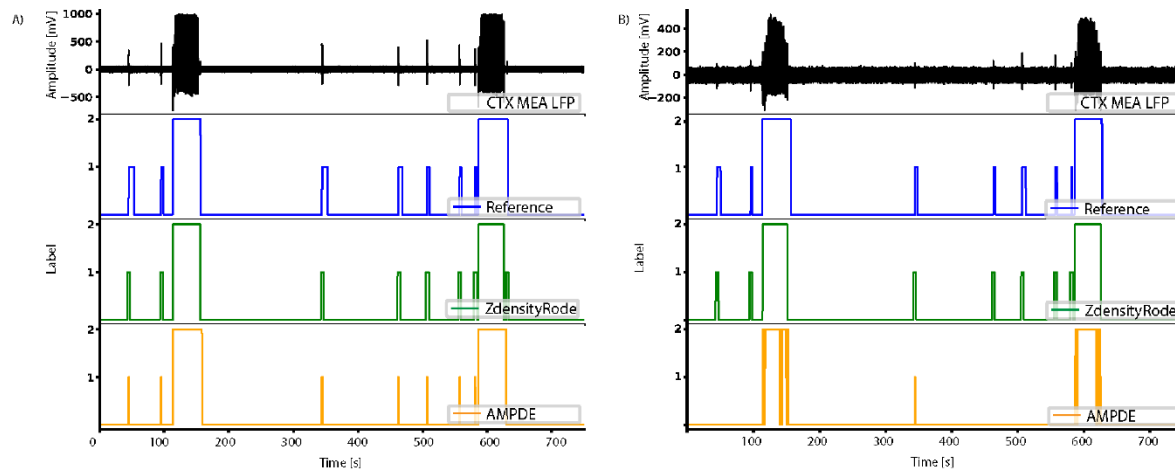


Figure 6. Example of semantic segmentation task through ZdensityRODE and AMPDE. Output comparison for ZdensityRode and AMPDE algorithms against reference annotations. Two sample signals have been used to showcase two different scenarios. A) shows a signal with a SNR higher than 20 dB whereas B) shows a signal with an SNR below 20 dB. The algorithm becomes less reliable with lower SNR. (0: baseline, 1: interictal event, 2: ictal event).

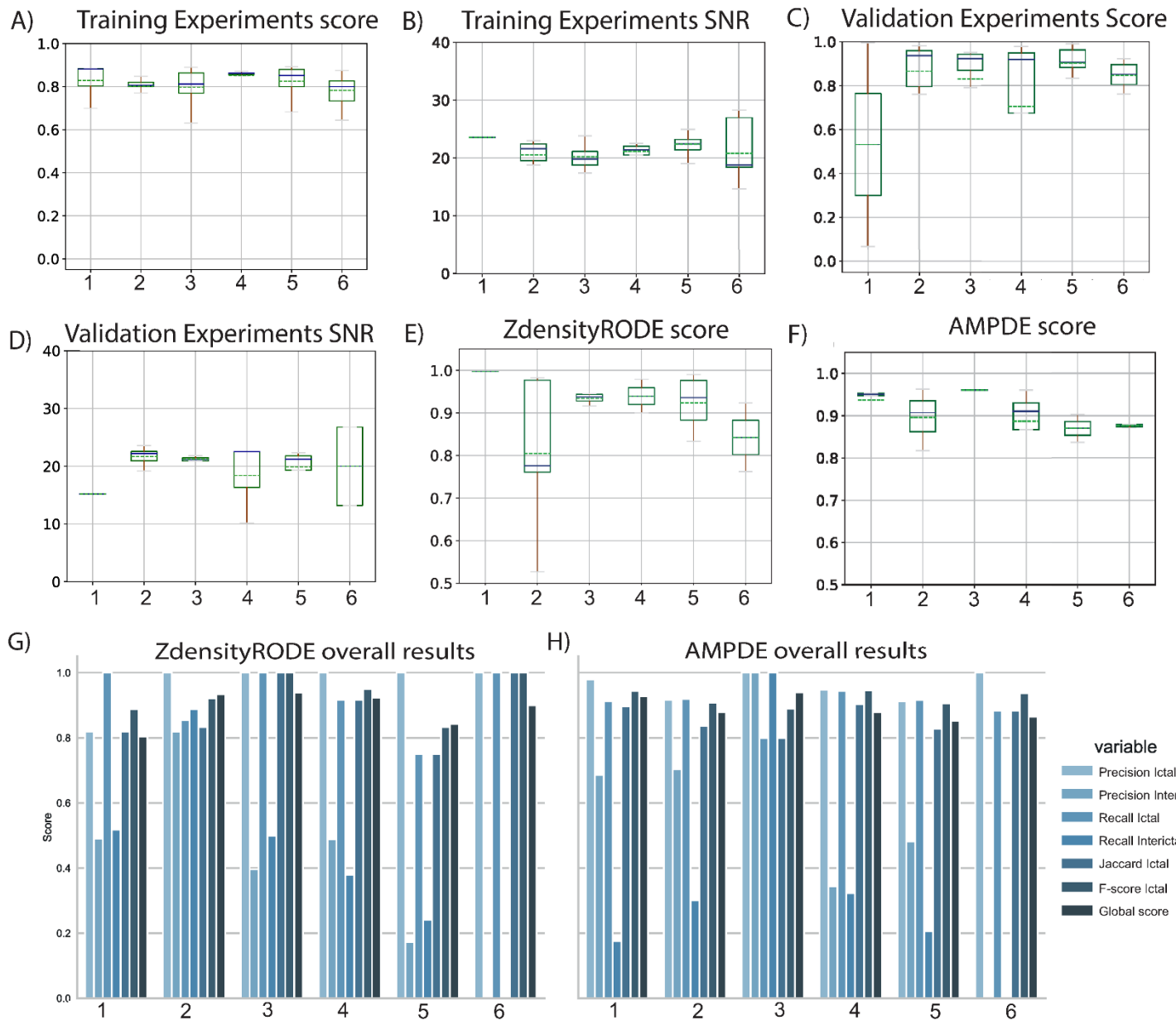


Figure 7. Experiments results. A) Distribution of scores for each experimental session in the training stage; B) Distribution of SNR for each experimental session in the training stage; C) Distribution of scores for the validation dataset; D) Distribution of SNR for the validation dataset; E) Distribution of scores for classifier ZdensityRODE; F) Distribution of scores for classifier AMPD; G) Scores for each metric used in the experiment for ZdensityRODE algorithm and H) Scores for each metric used for AMPD algorithm.

Code 1. Pseudo code for Z-score Density-based Robust Outlier Detection Estimation algorithm This pseudo code summarizes the algorithm stages by which it identifies and classifies the three different classes in the CTX MEA signal.

Algorithm 1 Brakkel Peak Classification

```

1: Input: signal
2: Input: lag ( $\lambda$ )
3: Input: influence ( $\iota$ )
4: Input: threshold ( $\tau$ )
5: Input: delta ( $\Delta$ )
6: Output: classified regions
7: Define an intermediary signal for filtered input values:  $U$ 
8: for  $x_i$  in signal do
9:   if Training stage then update buffers  $\mu$  and  $\sigma$  buffers
10:  else
11:    if  $(x_i - \mu_{i-1}) > threshold \cdot \sigma_{i-1}$  then
12:       $x_i$  is an outlier
13:       $U := (\iota \cdot x_i) + ((1 - \iota) * U_{i-1});$ 
14:    else  $U := x_i$ 
15:    end if
16:    avg := average(Chunk  $U$  for last  $\lambda$  samples);
17:    std := Standard deviation(Chunk  $U$  for last  $\lambda$  samples);
18:    for peak stored in processed window do
19:      Account number of peaks in a  $\Delta$  window
20:      if N peaks in  $\Delta$  time lapse  $\geq Threshold\_A$  then
21:        Classify interval as A label
22:      if  $Threshold\_B \leq N \leq Threshold\_A$  then
23:        Classify interval as B label

```

References

1. Falco-Walter J. Epilepsy—Definition, Classification, Pathophysiology, and Epidemiology. *Seminars in neurology*. 2020;40(6):617–623.
2. Galeote-Checa G, Nabaei V, Das R, Heidari H. Wirelessly powered and modular flexible implantable device. *ICECS 2020 - 27th IEEE International Conference on Electronics, Circuits and Systems, Proceedings*. 2020;doi:10.1109/ICECS49266.2020.9294856.
3. Ray TR, Choi J, Bandodkar AJ, Krishnan S, Gutruf P, Tian L, et al. Bio-integrated wearable systems: A comprehensive review. *Chemical Reviews*. 2019;119:5461–5533. doi:10.1021/ACS.CHEMREV.8B00573.
4. Ho JS, Kim S, Poon AS. Midfield wireless powering for implantable systems. *Proceedings of the IEEE*. 2013;101(6):1369–1378. doi:10.1109/JPROC.2013.2255221.
5. Galeote-Checa G, Panuccio G, Linares-Barranco B, Serrano-Gotarredona T. Baseline Features Extraction from Microelectrode Array Recordings in an in vitro model of Acute Seizures using Digital Signal Processing for Electronic Implementation. *2021 IEEE International Conference on Omni-Layer Intelligent Systems (COINS)*. 2021; p. 1–6. doi:10.1109/COINS51742.2021.9524089.

6. Burton A, Obaid SN, Vázquez-Guardado A, Schmit MB, Stuart T, Cai L, et al. Wireless, battery-free subdermally implantable photometry systems for chronic recording of neural dynamics. *Proceedings of the National Academy of Sciences of the United States of America*. 2020;117:2835–2845. doi:10.1073/PNAS.1920073117.
7. Yoo J, Yan L, El-Damak D, Altaf MAB, Shoeb AH, Chandrakasan AP. An 8-Channel Scalable EEG Acquisition SoC With Patient-Specific Seizure Classification and Recording Processor. *IEEE Journal of Solid-State Circuits*. 2013;48(1):214–228. doi:10.1109/JSSC.2012.2221220.
8. McGlynn E, Nabaei V, Ren E, Galeote-Checa G, Das R, Curia G, et al. The Future of Neuroscience: Flexible and Wireless Implantable Neural Electronics. *Advanced Science*. 2021;8. doi:10.1002/ADVS.202002693.
9. Geller EB, Skarpaas TL, Gross RE, Goodman RR, Barkley GL, Bazil CW, et al. Brain-responsive neurostimulation in patients with medically intractable mesial temporal lobe epilepsy. *Epilepsia*. 2017;58(6):994–1004. doi:<https://doi.org/10.1111/epi.13740>.
10. Zijlmans M, Jiruska P, Zelmann R, Leijten FS, Jefferys JG, Gotman J. High-Frequency Oscillations as a New Biomarker in Epilepsy. *Annals of Neurology*. 2012;71(2):169–178.
11. Fisher R, Salanova V, Witt T, Worth R, Henry T, Gross R, et al. Electrical stimulation of the anterior nucleus of thalamus for treatment of refractory epilepsy. *Epilepsia*. 2010;51(5):899–908.
12. Chvojka J, Kudlacek J, Chang WC, Novak O, Tomaska F, Otahal J, et al. The role of interictal discharges in ictogenesis - a dynamical perspective. *Epilepsy Behavior*. 2021;121:106591. doi:<https://doi.org/10.1016/j.yebeh.2019.106591>.
13. Topalovic U, Barclay S, Ling C, et al. A Wearable Platform for Closed-Loop Stimulation and Recording of Single-Neuron and Local Field Potential Activity in Freely Moving Humans. *Nature Neuroscience*. 2023;26:517–527. doi:10.1038/s41593-023-01260-4.
14. Page A, Sagedy C, Smith E, Attaran N, Oates T, Mohsenin T. A Flexible Multichannel EEG Feature Extractor and Classifier for Seizure Detection. *IEEE Transactions on Circuits and Systems II: Express Briefs*. 2015;62(2):109–113. doi:10.1109/TCSII.2014.2385211.
15. Cheng CH, Tsai PY, Yang TY, Cheng WH, Yen TY, Luo Z, et al. A Fully Integrated 16-Channel Closed-Loop Neural-Prosthetic CMOS SoC With Wireless Power and Bidirectional Data Telemetry for Real-Time Efficient Human Epileptic Seizure Control. *IEEE Journal of Solid-State Circuits*. 2018;53(11):3314–3326. doi:10.1109/JSSC.2018.2867293.
16. Park YS, Cosgrove GR, Madsen JR, Eskandar EN, Hochberg LR, Cash SS, et al. Early Detection of Human Epileptic Seizures Based on Intracortical Microelectrode Array Signals. *IEEE Transactions on Biomedical Engineering*. 2020;67(3):817–831. doi:10.1109/TBME.2019.2921448.
17. Aarabi A, He B. Seizure prediction in patients with focal hippocampal epilepsy. *Clinical Neurophysiology*. 2017;128(7):1299–1307. doi:<https://doi.org/10.1016/j.clinph.2017.04.026>.

18. Abdelhalim K, Smolyakov V, Genov R. Phase-Synchronization Early Epileptic Seizure Detector VLSI Architecture. *IEEE Transactions on Biomedical Circuits and Systems*. 2011;5(5):430–438. doi:10.1109/TBCAS.2011.2170686.
19. Imfeld K, Maccione A, Gandolfo M, Martinoia S, Farine PA, Koudelka-Hep M, et al. Real-time signal processing for high-density microelectrode array systems. *Wiley Online Library*. 2009;23:983–998. doi:10.1002/acs.1077.
20. Ahmadi-Farsani J, Linares-Barranco B, Serrano-Gotarredona T. Digital-signal-processor realization of izhikevich neural network for real-time interaction with electrophysiology experiments. *2019 26th IEEE International Conference on Electronics, Circuits and Systems, ICECS 2019*. 2019; p. 899–902. doi:10.1109/ICECS46596.2019.8965064.
21. Rajdev P, Ward MP, Rickus J, Worth R, Irazoqui PP. Real-time seizure prediction from local field potentials using an adaptive Wiener algorithm. *Computers in Biology and Medicine*. 2010;40(1):97–108. doi:<https://doi.org/10.1016/j.combiomed.2009.11.006>.
22. Avoli M, D'antuono M, Louvel J, Köhling R, Biagini G, Pumain R, et al. Network and pharmacological mechanisms leading to epileptiform synchronization in the limbic system in vitro. *Progress in Neurobiology*. 2002;68(3):167–207. doi:[https://doi.org/10.1016/S0301-0082\(02\)00077-1](https://doi.org/10.1016/S0301-0082(02)00077-1).
23. McIntyre DC, Gilby KL. Mapping seizure pathways in the temporal lobe. *Epilepsia*. 2008;49:23–30.
24. Bartolomei F, Khalil M, Wendling F, Sontheimer A, Régis J, Ranjeva JP, et al. Entorhinal cortex involvement in human mesial temporal lobe epilepsy: an electrophysiologic and volumetric study. *Epilepsia*. 2005;46(5):677–687.
25. Bartolomei F, Chauvel P, Wendling F. Epileptogenicity of brain structures in human temporal lobe epilepsy: a quantified study from intracerebral EEG. *Brain*. 2008;131(7):1818–1830.
26. Spencer SS, Spencer DD. Entorhinal-hippocampal interactions in medial temporal lobe epilepsy. *Epilepsia*. 1994;35(4):721–727.
27. Panuccio G, Colombi I, Chiappalone M. Recording and modulation of epileptiform activity in rodent brain slices coupled to microelectrode arrays. *JoVE (Journal of Visualized Experiments)*. 2018;(135):e57548.
28. Brakel JPGv. Robust peak detection algorithm using z-scores; 2014. <https://stackoverflow.com/questions/22583391/peak-signal-detection-in-realtime-timeseries-data/2264036222640362>. Available from: <https://stackoverflow.com/questions/22583391/peak-signal-detection-in-realtime-timeseries-data/22640362#22640362>.
29. Bishop SM, Ercole A. Multi-Scale Peak and Trough Detection Optimised for Periodic and Quasi-Periodic Neuroscience Data. *Acta Neurochir Suppl*. 2018;126:189–195. doi:10.1007/978-3-319-65798-1_39.
30. Scholkmann F, Boss J, Wolf M. An Efficient Algorithm for Automatic Peak Detection in Noisy Periodic and Quasi-Periodic Signals. *Algorithms*. 2012;5:588–603. doi:10.3390/a5040588.

31. Chung NC, Miasojedow B, Startek M, Gamin A. Jaccard/Tanimoto similarity test and estimation methods for biological presence-absence data. *BMC Bioinformatics*. 2019;20(Suppl 15):644. doi:10.1186/s12859-019-3118-5.
32. Gregg NM, Marks VS, Sladky V, Lundstrom BN, Klassen B, Messina SA, et al. Anterior nucleus of the thalamus seizure detection in ambulatory humans. *Epilepsia*. 2021;62(10):e158–e164.
33. Truong ND, Nguyen AD, Kuhlmann L, Bonyadi MR, Yang J, Ippolito S, et al. Convolutional neural networks for seizure prediction using intracranial and scalp electroencephalogram. *Neural Networks*. 2018;105:104–111. doi:<https://doi.org/10.1016/j.neunet.2018.04.018>.
34. Ronchini M, Zamani M, Huynh HA, Rezaeian Y, Panuccio G, Farkhani H, et al. A CMOS-based neuromorphic device for seizure detection from LFP signals. *Journal of Physics D: Applied Physics*. 2021;55(1):014001.
35. Ronchini M, Rezaeian Y, Zamani M, Panuccio G, Moradi F. NET-TEN: a silicon neuromorphic network for low-latency detection of seizures in local field potentials. *Journal of Neural Engineering*. 2023;20(3):036002.
36. Bin Altaf MA, Yoo J. A 1.83 μ J/Classification, 8-Channel, Patient-Specific Epileptic Seizure Classification SoC Using a Non-Linear Support Vector Machine. *IEEE Transactions on Biomedical Circuits and Systems*. 2016;10(1):49–60. doi:10.1109/TBCAS.2014.2386891.
37. Fisher RS, Vickrey BG, Gibson P, Hermann B, Penovich P, Scherer A, et al. The impact of epilepsy from the patient's perspective I. Descriptions and subjective perceptions. *Epilepsy Research*. 2000;41(1):39–51.
38. Haneef Z, Skrehot HC. Neurostimulation in Generalized Epilepsy: A Systematic Review and Meta-Analysis. *Epilepsia*. 2023;
39. Galeote-Checa G, Panuccio G, Linares-Barranco B, Serrano-Gotarredona T. Baseline Features Extraction from Microelectrode Array Recordings in an in vitro model of Acute Seizures using Digital Signal Processing for Electronic Implementation. 2021 IEEE International Conference on Omni-Layer Intelligent Systems, COINS 2021. 2021;doi:10.1109/COINS51742.2021.9524089.
40. de Curtis M, Jefferys JG, Avoli M. Interictal epileptiform discharges in partial epilepsy. *Jasper's Basic Mechanisms of the Epilepsies* [Internet] 4th edition. 2012;
41. Staba RJ, Stead M, Worrell GA. Electrophysiological Biomarkers of Epilepsy. *Neurotherapeutics*. 2014;11(2):334–46. doi:10.1007/s13311-014-0259-0.
42. Jacobs J, Staba R, Asano E, Otsubo H, Wu JY, Zijlmans M, et al. High-frequency oscillations (HFOs) in clinical epilepsy. *Progress in Neurobiology*. 2012;98(3):302–315. doi:<https://doi.org/10.1016/j.pneurobio.2012.03.001>.
43. Khan YU, Farooq O, Sharma P. Automatic detection of seizure onset in pediatric EEG. *International Journal of Embedded Systems and Applications*. 2012;2(3):81–89.
44. Shoaran M, Hagh BA, Taghavi M, Farivar M, Emami-Neyestanak A. Energy-Efficient Classification for Resource-Constrained Biomedical Applications. *IEEE Journal on Emerging and Selected Topics in Circuits and Systems*. 2018;8(4):693–707. doi:10.1109/JETCAS.2018.2844733.

45. Ahammad N, Fathima T, Joseph P, et al. Detection of epileptic seizure event and onset using EEG. *BioMed research international*. 2014;2014.
46. Huang SA, Chang KC, Liou HH, Yang CH. A 1.9-mW SVM processor with on-chip active learning for epileptic seizure control. *IEEE Journal of Solid-State Circuits*. 2019;55(2):452–464.
47. Shoeb AH, Gutttag JV. Application of machine learning to epileptic seizure detection. In: *Proceedings of the 27th international conference on machine learning (ICML-10)*; 2010. p. 975–982.
48. Das K, Daschakladar D, Roy PP, Chatterjee A, Saha SP. Epileptic seizure prediction by the detection of seizure waveform from the pre-ictal phase of EEG signal. *Biomedical Signal Processing and Control*. 2020;57:101720. doi:10.1016/J.BSPC.2019.101720.
49. De Cooman T, Vandecasteele K, Varon C, Hunyadi B, Cleeren E, Van Paesschen W, et al. Personalizing heart rate-based seizure detection using supervised SVM transfer learning. *Frontiers in Neurology*. 2020;11:145.
50. Birjandtalab J, Jarmale VN, Nourani M, Harvey J. Impact of Personalization on Epileptic Seizure Prediction. In: *2019 IEEE EMBS International Conference on Biomedical Health Informatics (BHI)*; 2019. p. 1–4.
51. He J, Liu D, Chen X. Wearable exercise electrocardiograph signal quality assessment based on fuzzy comprehensive evaluation algorithm. *Computer Communications*. 2020;151:86–97. doi:<https://doi.org/10.1016/j.comcom.2019.12.051>.
52. Satija U, Ramkumar B, Manikandan MS. A Review of Signal Processing Techniques for Electrocardiogram Signal Quality Assessment. *IEEE Reviews in Biomedical Engineering*. 2018;11:36–52. doi:10.1109/RBME.2018.2810957.